CSCanada
Energy Science and Technology
Vol. 5, No. 1, 2013, pp. 1-16
DOI:10.3968/j.est.1923847920130501.854

ISSN 1923-8460[PRINT]
ISSN 1923-8479[ONLINE]
www.cscanada.net
www.cscanada.org

Performance Model of a Regenerative Hydrogen Bromine Fuel Cell for Grid-Scale Energy Storage

Brian Huskinson[a]; Michael J. Aziz[a],*

[a] Harvard School of Engineering and Applied Sciences, 29 Oxford Street, Cambridge, MA.
* Corresponding author

Supported by National Science Foundation grant NSF-IIP-0848366 through Sustainable Innovations, LLC.

Received 14 February 2013; accepted 26 February 2013

Abstract

We develop a performance model for a polymer electrolyte membrane based regenerative hydrogen-bromine fuel cell (rHBFC). The model includes four voltage loss mechanisms: ohmic loss through the membrane, hydrogen electrode activation, bromine electrode activation, and bromine electrode mass transport. We explore a large parameter space by looking at the dependences of each of these losses as a function of two "operating parameters", acid concentration and temperature; and five "engineering parameters", bromine electrode exchange current density, hydrogen electrode exchange current density, membrane thickness, diffusion layer thickness, and hydrogen gas pressure. The relative importance of each of the losses is explored as both the engineering parameters and operating parameters are varied. The model is also compared to published experimental results on the performance of a hydrogen-bromine cell. By varying engineering parameters and operating parameters within plausible ranges, we project that, with further research, a cell of this design could be developed that operates at greater than 90% voltage efficiency at current densities $>$ 700 mA cm^{-2} in both electrolytic and galvanic modes and that has a peak galvanic power density of 2760 mW cm^{-2}.

Key words: Energy storage; Regenerative hydrogen-bromine fuel cell; Electrolytic and galvanic modes

Huskinson, B., & Aziz, M. J. (2013). Performance Model of a Regenerative Hydrogen Bromine Fuel Cell for Grid-Scale Energy Storage. *Energy Science and Technology*, *5*(1), 1-16. Available from: URL: http://www.cscanada.net/index.php/est/article/view/10.3968/j.est.1923847920130501.854
DOI: http://dx.doi.org/10.3968/j.est.1923847920130501.854

LIST OF SYMBOLS

A	Arrhenius pre-exponential factor, Ω^{-1} cm^{-1}
a_{Br_2}	Activity of aqueous bromine
a_{H_2}	Activity of hydrogen gas
$a_{HBr(aq)}$	Activity of hydrobromic acid
c_{Br_2}	Concentration of bromine, mol L^{-1}
c_{HBr}	Concentration of hydrobromic acid, mol L^{-1}
C_O^{bulk}	Bulk concentration of oxidized form (Br_2), mol cm^{-3}
C_O^S	Concentration of oxidized form (Br_2) near the electrode surface, mol cm^{-3}
C_R^{bulk}	Bulk concentration of reduced form (Br^-), mol cm^{-3}
C_R^S	Concentration of reduced form (Br^-) near the electrode surface, mol cm^{-3}
D	Diffusion coefficient, cm^2 s^{-1}
D_{Br^-}	Diffusion coefficient of Br^-, cm^2 s^{-1}
D_{Br_2}	Diffusion coefficient of Br_2, cm^2 s^{-1}
E	Cell potential, V
E_a	Arrhenius activation energy, kcal mol^{-1}
E_0'	Standard cell potential, V
E_{eq}	Equilibrium potential, V
$E_{eq,ideal}$	Equilibrium potential, V
$E_{eq,Nernst}$	Equilibrium potential, V
$E_{eq,Yeo}$	Equilibrium potential, V
f_{H_2}	Fugacity of hydrogen gas, atm
i	Cell current density, mA cm^{-2}
i_0^{Br}	Bromine electrode exchange current density, mA cm^{-2}
i_0^H	Hydrogen electrode exchange current density, mA cm^{-2}
J	Diffusive flux of species, mol cm^{-2} s^{-1}
l	Proton-exchange membrane thickness, μm
m	Molality, mol kg^{-1}
M	Molarity, mol L^{-1}
p	Cell power density, mW cm^{-2}
p_{H2}	Hydrogen gas partial pressure, atm
T	Temperature, degrees Celsius
X	Weight fraction of HBr in solution
Greek letters	
α	Transfer coefficient
γ_{Br_2}	Activity coefficient of Br_2(aq)
γ_{HBr}	Activity coefficient of HBr(aq)
γ_{H_2}	Activity coefficient of H_2
ΔC	Concentration gradient across diffusion layer, mol cm^{-3}
Δx	Diffusion layer thickness, equivalent to ε, cm
ε	Diffusion layer thickness, cm
η	Cell efficiency

η_{Br}	Total bromine electrode activation overpotential (including mass transport effects), V
η_{Br},	Concentration-independent bromine electrode activation overpotential, V
η_H	Hydrogen electrode activation overpotential, V
η_{MT}	Bromine electrode mass transport overpotential, V
η_R	Resistive overpotential, V
μ	Viscosity, mPa · s or cP
ν	Kinematic viscosity, $m^2\ s^{-1}$
ρ_{H_2O}	Density of water, g L^{-1}
ρ_{HBr}	Density of hydrobromic acid, g L^{-1}
σ	Membrane conductivity, $\Omega^{-1}\ cm^{-1}$
ϕ	Variable from Yeo and Chin, V
Constants	
A_ρ	ρ_{HBr} fit, 59.98
B_ρ	ρ_{HBr} fit, -0.1300
c_0	Reference concentration, 1 M
C_ρ	ρ_{HBr} fit, 0.001061
D_ρ	ρ_{HBr} fit, -1.263
E_ρ	ρ_{HBr} fit, 0.02160
F	Faraday's constant, 96485 C mol^{-1}
F_ρ	ρ_{HBr} fit, -0.0001647
MW_{H_2O}	Molecular weight of H_2O, 18.0153 g mol^{-1}
MW_{HBr}	Molecular weight of HBr, 80.91 g mol^{-1}
n	Number of moles of electrons transferred in reaction, 2
p_0	Reference pressure, 1 atm
R	Ideal gas constant, 8.314 J $mol^{-1}\ K^{-1}$ or 0.0019859 kcal $mol^{-1}\ K^{-1}$
u_0	Free stream fluid velocity, 0.1 m s^{-1}
V_1	Molecular volume of solute (53.2 for Br_2, 27 for Br^-), $cm^3\ mol^{-1}$
V_2	Molecular volume of solvent (18.9 for H_2O), $cm^{-3}\ mol^{-1}$
x	Distance downstream from beginning of boundary layer, 10 μm

INTRODUCTION

Flow batteries are of increasing interest for applications in grid scale energy storage, particularly batteries with high energy capacities suited for balancing the intermittent nature of wind and solar photovoltaic power production (Mellentine, Culver, & Savinell, 2011; Eyer & Corey, 2010; Rugolo & Aziz, 2012; Kondoh, Ishii, Yamaguchi, & Murata, 2000; Ibrahim, Ilinca, & Perron, 2008). Flow batteries and regenerative fuel cells maintain a modular separation between the power elements of the system (the cell stack) and the energy elements of the system (the reactant and product storage tanks), permitting independent scaling of the two. This is in contrast to many conventional battery technologies, where the power and energy components of the system scale together, thereby making it difficult to scale these systems to grid-level storage (Weber *et al.*, 2011; Nguyen & Savinell, 2010). Halogen-based devices, like that discussed here, are promising due to rapid charge-transfer kinetics associated with the electrode reaction, thereby permitting high efficiency operation. The device discussed here is bromine-based, but we note that work using another halogen – chlorine – has also demonstrated good device performance (Anderson, Taylor, Wilemski, & Gelb, 1994; Chin, Yeo, McBreen, & Srinivasan, 1979; Gileadi *et al.*, 1977; Mondal, Rugolo, & Aziz, 2011; Rugolo, Huskinson, & Aziz, 2012; Thomassen, Børresen, Hagen, & Tunold, 2003; Thomassen, Sandnes, Børresen, & Tunold, 2006; Yeo, McBreen, Tseung, Srinivasan, & McElroy, 1980). The regenerative hydrogen-bromine fuel cell (rHBFC) is an energy storage device that facilitates the following electrochemical reaction:

$$H_2(g) + Br_2(aq) \rightleftharpoons 2HBr(aq) \quad (1)$$

In discharge (galvanic) mode, H_2 and Br_2 react to produce electricity and HBr(aq). In charge (electrolytic) mode, electricity is consumed to split HBr(aq) into H_2 and Br_2, which is then stored in tanks until the electricity is needed (figure 1).

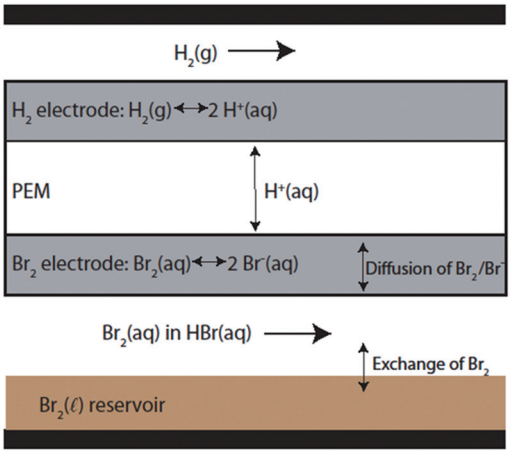

Figure 1
A Schematic of a Regenerative Hydrogen-Bromine Fuel Cell

In charge or electrolytic mode, hydrobromic acid is electrolyzed to produce hydrogen and bromine using electrical energy from an external source. The products are stored in tanks for future re-conversion to electricity. In discharge or galvanic mode, hydrogen and bromine react to produce hydrobromic acid and electricity.

Earlier studies on hydrogen-bromine electrochemical devices demonstrated promising performance. In a study by Yeo and Chin (1980), round-trip electric-to-electric efficiencies were reported at about 70% for current densities between 150 to 225 mA cm^{-2}, depending on the electrolyte composition, with the cell capable of operation to at least 300 mA cm^{-2}. Soon after, work on HBr electrolyzers led to devices capable of operating around 330 mA cm^{-2} in electrolytic mode (Balko, McElroy, & Laconti, 1981). In more recent work, Livshits *et al.* (2006) reported current densities in excess of 2400 mA cm^{-2}, with the cell power density exceeding 1500 mW cm^{-2} at 80 ˚C, by utilizing a novel, non-standard membrane. Kreutzer *et al.* (2012) achieved power densities exceeding 450 mW cm^{-2} near 750 mA cm^{-2} (at 45 ˚C) for a cell utilizing a standard Nafion membrane. Modeling the performance of hydrogen-bromine systems has been done before (Savinell & Fritts, 1988; Yeo & Chin, 1980), with the most developed model coming from Savinell *et al.* Our model differs from previous work in two key ways: (1) we include the effects of temperature on equilibrium potentials, membrane resistances, electrode activation kinetics, and mass transport of species to and

from the electrode surface, and (2) we systematically vary the cell operating parameters, such as temperature and electrolyte composition, while also varying cell engineering parameters, discussed below, to identify performance "sweet spots." The large parameter space we explore is unrivaled in the literature. In exploring this large parameter space, certain simplifications were made (such as effectively reducing the mass transport behavior to a single engineering parameter) that allow us to explore a very broad range of possible cell characteristics, e.g. examining a cell with severe mass transport limitations vs. a cell with minimal mass transport limitations. This was done so that this model could be used as a guide to future R&D efforts, helping to identify aspects of the cell performance that demand the most attention.

1. THE MODEL

The purpose of this model is to determine the cell potential (in volts) as a function of current density (in mA cm^{-2}) for a given set of operating parameters (OPs: temperature and electrolyte composition) and engineering parameters (EPs: electrode exchange current densities, membrane thickness, diffusion layer thickness, and H_2 gas pressure). In this study, we consider the EPs and OPs as well as the dependent physical properties that determine cell losses, such as proton exchange membrane (PEM) conductivity, electrode kinetics, and bromine/bromide mass transport in solution. Our objectives are to predict cell voltage efficiency and cell power density p as functions of current density and to determine how these functions change as we vary both the OPs and the EPs. The model was used to evaluate cell potentials in both charge mode and discharge mode, but for the majority of results presented here, we omit the electrolytic, charge-mode behavior. Typically, a cell that shows good performance in discharge mode also shows good performance in charge mode (particularly within the confined concentration range used in this model), allowing us to simplify the presentation of the model results. We primarily consider two different sets of EPs: a "Base Case" with relatively conservative values for the EPs, which should be attainable today, and a "More Optimal Case" that uses more optimistic values that should be attainable with further research and development. Justifications for the values of each of these parameters are provided in the relevant subsections of this article. The energy conversion efficiency of the cell is the product of the voltage efficiency and the coloumbic efficiency, and the round-trip efficiency of the device is the product of the energy conversion efficiency in galvanic mode and the energy conversion efficiency in electrolytic mode. The primary coloumbic loss is via reactant crossover through the membrane, which we discuss later. If this loss is small enough, then the energy conversion efficiency is indistinguishable from the voltage efficiency. The voltage efficiency of the cell is a function of the current density i, with one expression for the galvanic direction and a different one for the electrolytic direction. In the galvanic case (which we take as defining positive i), hydrogen and bromine react to produce hydrobromic acid and electricity. The voltage efficiency is the electrical energy per charge produced (the cell potential $E(i)$), divided by the electrical energy per charge that could be produced reversibly (the equilibrium potential E_{eq}). In the electrolytic case (negative i), electrical energy is supplied to split HBr(aq) into H_2 and Br_2 for energy storage. Here, the voltage efficiency is the maximum possible electrical energy returned per charge stored, E_{eq}, divided by the electrical energy per charge spent in doing the electrolysis, $E(i)$:

$$\text{cell voltage efficiency} = \begin{cases} \dfrac{E(i)}{E_{eq}} : i \geq 0 \quad (galvanic) \\ \dfrac{E_{eq}}{E(i)} : i \leq 0 \quad (electrolytic) \end{cases} \tag{2}$$

The power density (in mW cm^{-2}) is the amount of power produced per cell area. It is equal to the cell potential multiplied by the current density:

$$p = i \cdot E(i). \tag{3}$$

Because of the high cost of fuel cells per unit cell area, cells having high efficiencies at large power densities are desirable. The cell potential deviates from its equilibrium value due to several loss mechanisms, all of which lead to the generation of heat in the cell. We identify four overpotentials in the cell: the hydrogen and bromine electrode overpotentials (η_H and η_{Br}; the latter actually includes two losses: one due to electrode activation and one due to mass transport limitations at the bromine electrode), and the membrane resistance overpotential (η_R). Each overpotential is a function of current density and depends on the OPs and a subset of the EPs. The overall cell potential can thus be expressed as the equilibrium cell potential minus the individual losses:

$$E(i) = E_{eq} - \eta_R(i) - \eta_H(i) - \eta_{Br}(i), \tag{4}$$

where all of the above quantities are in volts. E_{eq} is a function of temperature and of the activities of the reactants and products, which themselves depend on temperature and concentration. η_R is determined by the conductance of the membrane, which depends on temperature, acid concentration, and membrane thickness. The overpotentials at the two electrodes arise from two different effects: an activation loss due to the kinetics involved with the electron transfer at the surface, and a mass transport loss due to the depletion of the reactants and enrichment of the products near the electrode surface at non-zero current densities. We ignore the mass transport effect at the hydrogen electrode due to presumed fast transport of gaseous hydrogen, whereas we include the bromine mass transport because of the relatively slow transport of Br_2(aq) in aqueous solution. This overpotential is denoted η_{MT}.

1.1 The Equilibrium Potential

The equilibrium potential is that of the combined half-cell reactions, where all potentials are relative to that of a standard hydrogen electrode (SHE):

$$H_2(g) \rightleftharpoons 2H^+(aq) + 2e^- \quad E_{eq} = 0.000 \quad V \tag{5}$$

$$Br_2(aq) + 2e^- \rightleftharpoons 2Br^-(aq) \quad E_{eq} = 1.087 \quad V. \tag{6}$$

The equilibrium potential can be described by the Nernst equation:

$$E_{eq,Nernst} = E_0^{'} + \frac{R(T+273.15)}{nF} \ln\left(\frac{a_{Br_2} a_{H_2}}{a_{HBr(aq)}^2}\right), \tag{7}$$

where R = 8.314 J mol K^{-1} is the universal gas constant, T is the temperature (in ˚C), n is the number of electrons transferred in the reaction (n=2 here), and F = 96485 C mol^{-1} is Faraday's constant. The activities of Br_2, HBr and H_2 are denoted a_{Br_2}, a_{HBr}, and a_{H_2}, respectively. They are defined by the following equations:

$$a_{Br_2} = \frac{\gamma_{Br_2} c_{Br_2}}{c_0}, \tag{8}$$

and

$$a_{HBr} = \frac{\gamma_{HBr} c_{HBr}}{c_0}, \tag{9}$$

and

$$a_{H_2} = \frac{\gamma_{H_2} p_{H_2}}{p_0}, \tag{10}$$

where a_{Br_2} and a_{HBr} are the concentrations of Br_2 and HBr, respectively (in molarity, M), c_0 is the standard concentration of 1 M, p_{H_2} is the H_2 gas pressure, p_0 is the standard pressure of 1 atm, and γ_{Br_2}, γ_{HBr}, and γ_{H_2} are the activity coefficients of Br_2, HBr, and H_2, respectively. $E_0^{'}$ is the temperature-dependent equilibrium potential when all activities are unity. $E_0^{'}$ must be chosen so that E_{eq} = 1.087 V at the standard temperature, pressure, and concentration of 25 ˚C, 1 atm, and 1 M, respectively. Assuming the difference between reactant and product entropies is independent of temperature, $E_0^{'}$ is a linear function of temperature, whose slope is given by the entropy of formation divided by 2F (Lide, 2005; Lide, 2011):

$$E'_0 = 1.2679 - 0.0006105(T + 273.15) \tag{11}$$

This equation can then be substituted into the Nernst equation to provide a full expression for the cell equilibrium potential:

$$E_{eq,Nernst} = 1.2679 - 0.0006105(T + 273.15) + \frac{RT}{2F} \ln\left(\frac{a_{Br_2} a_{H_2}}{a_{HBr(aq)}^2}\right) \tag{12}$$

1.1.1 Calculating $E_{eq,ideal}$

One method of approximating the equilibrium potential involves using Equation 12 and setting all of the activity coefficients equal to unity. This procedure provides what we term the "ideal" equilibrium potential, $E_{eq,ideal}$, with the following form:

$$E_{eq,ideal} = 1.2793 - 0.0006104(T + 273.15) + \frac{RT}{2F} \ln\left(\frac{[Br_2][H_2]}{[HBr(aq)]^2}\right) \tag{13}$$

where $[Br_2]$ and $[HBr(aq)]$ represent the normalized concentrations of bromine and hydrobromic acid (i.e. $[Br_2] = c_{Br_2} / c_0$ and $[HBr] = c_{HBr} / c_0$) and $[H_2]$ represents the normalized pressure of H_2 gas (i.e. $[H_2] = p_{H_2} / p_0$).

1.1.2 Calculating $E_{eq,Yeo}$ Using a Semi-Empirical Expression

Another way we calculate the equilibrium potential is to use a semi-empirical expression from Yeo and Chin (1980). The expression takes the following form:

$$E_{eq,Yeo} = \phi - (T-25)\left(4.3 + 1.86 \cdot ln\frac{12.36X}{1-X}\right) \cdot 10^{-4} + 4.31 \cdot 10^{-5} \cdot T\left(ln \quad f_{H_2} + ln \quad a_{Br_2}\right) \tag{14}$$

where X is the weight fraction of HBr in solution, f_{H2} is the fugacity of H_2 gas, and ϕ takes the following form:

$$\phi = \begin{cases} 1.073 - 0.0567 \cdot ln\dfrac{12.36X}{1-X}, & if \ \ 0.016 < X < 0.11 \\ 1.095 - 0.1042 \cdot ln\dfrac{12.36X}{1-X}, & if \ \ 0.11 < X < 0.28 \\ 1.336 - 0.2581 \cdot ln\dfrac{12.36X}{1-X}, & if \ \ 0.28 < X < 0.58 \end{cases} \tag{15}$$

To compute the weight fraction of HBr in solution, X, we use the following expression:

$$X = \frac{MW_{HBr} M}{\rho_{HBr}} \tag{16}$$

where MW_{HBr} is the molecular weight of HBr (80.91 g mol^{-1}), M is the molarity of HBr (in mol L^{-1}), and ρ_{HBr} is the density of HBr(aq) (in g L^{-1}). The density itself is a function of temperature and concentration, and has been presented in empirical form by Novotný and Söhnel (1988):

$$\rho_{HBr(aq)} = \rho_{H_2O} + A_\rho M + B_\rho MT + C_\rho MT^2 + D_\rho M^{3/2} + E_\rho M^{3/2} T + F_\rho M^{3/2} T^2 \tag{17}$$

where the temperature-dependent density of water, ρ_{H_2O} (in g L^{-1}) is given by the empirical expression:

$$\rho_{H_2O} = 999.65 + 0.20438T - 0.06174T^{3/2}. \tag{18}$$

The parameters are as follows: A_ρ = 59.98, B_ρ = -0.1300, C_ρ = 0.001061, D_ρ = -1.263, E_ρ = 0.02160, and F_ρ = -0.0001647, each having units necessary to give their respective terms density units of g L^{-1}. This expression for the equilibrium potential from Yeo and Chin is in some

sense the most useful, as it accounts for a lot of non-ideal behavior because it is a semi-empirical expression based on real cell measurements. Importantly, $E_{eq,Yeo}$ and $E_{eq,ideal}$ vary significantly from one another. Figure 2 highlights this, showing calculated curves for $E_{eq,Yeo}$ and $E_{eq,ideal}$ at 5 ˚C, 25 ˚C, and 75 ˚C. For subsequent calculations in this article, $E_{eq,Yeo}$ is used to represent the cell equilibrium potential.

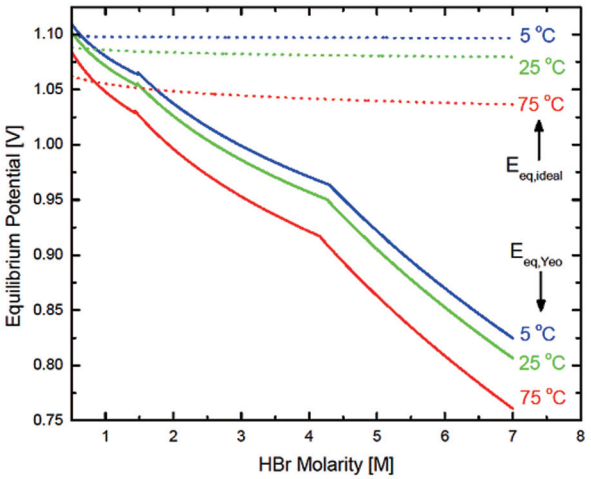

Figure 2
Equilibrium Potential vs. HBr Molarity at 5 ˚C, 25 ˚C, and 75 ˚C, Calculated Using Equations 13 ($E_{eq,ideal}$, Dotted Lines) and 14 ($E_{eq,Yeo}$, Solid Lines)
Strong deviations from ideality are seen at high acid concentrations for $E_{eq,Yeo}$. The three "tiers" seen in $E_{eq,Yeo}$ result from the definition of Φ in Equation 15.

1.2 The Membrane Resistance Overpotential, η_R

The resistance of the proton exchange membrane is very important in determining the operational characteristics of a hydrogen-bromine cell. The membrane conductance depends on the thickness of the membrane and the membrane conductivity, which is itself a function of temperature and acid concentration. The membrane conductivity is assumed to be independent of the membrane thickness and of the Br_2 concentration in solution. The resistance overpotential is calculated as follows:

$$\eta_R = \frac{l}{\sigma}\frac{i}{1000} \tag{19}$$

where l is the membrane thickness (in cm), σ is the membrane conductivity (in Ω^{-1} cm^{-1}), i is the current density (in mA cm^{-2}), and η_R is the resistive overpotential (in volts). The factor of 1000 assures consistency in units. Commercial DuPont Nafion membranes are typically available in thicknesses ranging from 25 to 250 μm. In the Base Case presented here, a value of 125 μm is used for the membrane thickness (equivalent to Nafion 115). The More Optimal case uses a 25 μm thick membrane. From a voltage loss perspective, it always helps to decrease the thickness of the membrane, though this can only be done to a certain extent in practice: mechanical integrity of the membrane is very important, as membrane rupture would allow the uncontrolled mixing and reaction of H_2 and Br_2. Furthermore, reactant crossover increases with the use of thinner membranes, lowering the current efficiency of the cell. Thus, the membrane thickness is also practically limited by the degree of reactant crossover that can be tolerated in a given system. Yeo and McBreen (1979) measured the extent of bromine crossover under a variety of electrolyte concentrations. Steady-state crossover current densities were reported as high as 3.57 mA/cm^2 for Br_2 in 12% HBr and as low as 0.0135 mA/cm^2 for Br_2 in 48% HBr for a Nafion 120 (250 μm thick) membrane. Assuming the crossover is inversely proportional to the membrane thickness, this would result in crossover current densities ranging from 0.135 mA cm^{-2} to 35.7 mA cm^{-2} in a 25 μm thick membrane, or 0.027 mA cm^{-2} to 7.14 mA cm^{-2} in a 125 μm thick membrane. The upper end of this range would represent a significant coloumbic loss in a real cell, while the lower end would essentially be negligible. Further experimental studies are necessary to determine which end of this range is more applicable to cells of interest, and considerations of the crossover current density are essential in determining the ideal operating conditions (especially HBr/Br_2 concentrations) for this type of cell. The membrane conductivity is a complicated function of both HBr(aq) concentration and temperature. Data from both Baldwin (1987) and Sone *et al.* (1996) were used for the calculations here, with the latter providing activation energies for proton conduction in Nafion in pure water (i.e. 0 M acid). The conductivity is assumed to take on an Arrhenius form:

$$\sigma(M,T) = A(M)e^{\frac{-E_a(M)}{RT}} \tag{20}$$

where A(M) is a pre-exponential factor (in Ω^{-1} cm^{-1}) and $E_a(M)$ is an activation energy (in kcal mol^{-1}). Baldwin provides data for σ and E_a at five different molarities ranging from 1.34 M HBr to 7.32 M HBr (a total of 23 data points). Sone *et al.* provide data for σ and E_a at 0 M HBr (i.e. Nafion in pure water). Using these values, the pre-exponential factor A can be calculated for the six molarities studied in these references. Now, having values for A(M) and $E_a(M)$ at six different molarities, Equation 20 can be used to calculate values for σ at any given temperature for each of the six molarities. A spline interpolation was then done in Matlab using the six curves drawn from Equation 20, so that σ could be calculated for an arbitrary value of the acid concentration between 0 M and 7.32 M. Figure 3 shows the membrane conductivity as a function of HBr molarity at a variety of temperatures. A subset of the data from Baldwin is included to indicate the quality of the fits. Notice that, at 5 ˚C, the conductivity experiences a local maximum near 4 M and a local minimum near 2 M. As the temperature is increased, the local maximum shifts to lower concentrations, and the local minimum disappears altogether, consistent with data

from Baldwin. For temperatures ≥ 50 ˚C, the conductivity peaks near 2 M.

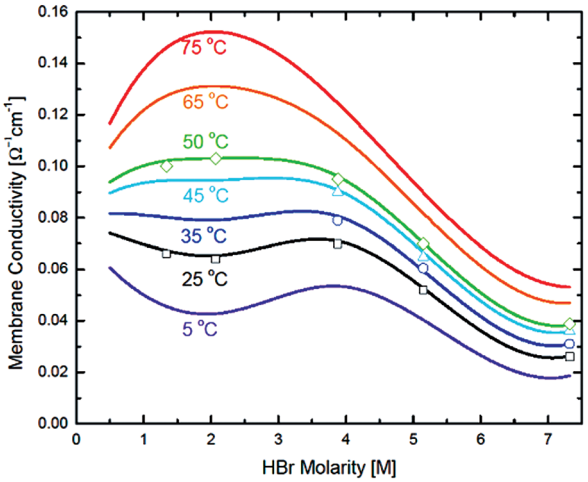

Figure 3
Membrane Conductivity vs. Acid Molarity at Several Different Temperatures, Calculated Using Data from Both Baldwin and Sone *et al.*
The data points shown are a subset of those provided by Baldwin (1987).

1.3 The Hydrogen Electrode Overpotential, η_H

The activation overpotential at the hydrogen electrode, η_H (in volts), is defined using a concentration-independent form of the Butler-Volmer equation:

$$i = i_0^H \left[\exp\left(\frac{-\alpha F \eta_H}{RT} \right) - \exp\left(\frac{(1-\alpha) F \eta_H}{RT} \right) \right] \qquad (21)$$

where i_0^H is the exchange current density of the structured hydrogen electrode (in mA cm^{-2}) and α is the transfer coefficient (Bard & Faulkner, 2001). We neglect the effects of mass transport at the hydrogen electrode due to presumed fast transport of H_2 gas. For the model, we set the value of the transfer coefficient for both electrodes equal to 0.5. We invert Equation 21 numerically to obtain η_H as a function of i. One important consideration is that the real surface area of the electrode is typically different, and often vastly different, than the projected surface area of the electrode. In a PEM fuel cell, electrodes are usually made up of finely dispersed catalyst particles that have a collective surface area much larger than the geometric area of the electrode. Technically, i_0 may also depend on temperature, but we ignore this dependence because of the uncertainty in the catalytic activity and because the area multiplier is much more significant. The exchange current density of real hydrogen electrodes has been studied in detail in the context of hydrogen-oxygen PEM fuel cells. Neyerlin *et al.* (2007) report that for a structured fuel cell electrode, the increase in the effective hydrogen exchange current density over that of a single crystal surface can be as large as a factor of 500. They measured i_0^H values in the range 250-600 mA cm^{-2}. For the Base Case in this study, we set i_0^H equal to 250 mA cm^{-2}, and for the More Optimal Case, we set i_0^H equal to 600 mA cm^{-2}, based on these measurements. Note that all of the exchange current densities used in the model refer to structured electrodes with real surface areas considerably higher than the projected surface areas of the electrodes.

1.4 The Bromine Electrode Overpotential, η_{Br}

In galvanic mode, the consumption of Br_2 and production of Br^- result in a depletion of Br_2 near the electrode and an enrichment of Br^-. The opposite occurs in electrolytic mode. For a given current density, the transport behavior of the system stabilizes at a steady-state concentration of reactant and product, so long as there exists a boundary somewhere in the system with a stable concentration and enough time is allowed to reach this steady state. In this case, we can express the concentrations of Br_2 and Br^- near the electrode as functions of current density. The full, concentration-dependent Butler-Volmer equation describes the total bromine electrode overpotential:

$$i = i_0^{Br} \left[\frac{C_O^s(i)}{C_O^{bulk}} \exp\left(\frac{-\alpha F \eta_{Br}}{RT} \right) - \frac{C_R^s(i)}{C_R^{bulk}} \exp\left(\frac{(1-\alpha) F \eta_{Br}}{RT} \right) \right], \qquad (22)$$

where C_O^{bulk} and C_R^{bulk} are the bulk concentrations of the oxidized and reduced forms, respectively, $C_O^s(i)$ and $C_R^s(i)$ are their respective concentrations near the electrode surface (all in mol cm^{-3}), and i_0^{Br} is the bromine electrode exchange current density (in mA cm^{-2}). The oxidized form is Br_2 and the reduced form is Br^-. Values approaching 200 mA cm^{-2} for i_0^{Br} have been measured on structured commercial Pt/C electrodes with loadings of about 0.55 mg Pt cm^{-2} (Kreutzer, Yarlagadda, & Van Nguyen, 2012). Values for i_0^{Br} on vitreous carbon are closer to 40 mA cm^{-2}, based on estimates by Savinell *et al.* (1988), with this estimate based on work by White *et al.* (1983) and Mastragostino *et al.* (1985). In our model, the bromine electrode exchange current density is set to 40 mA cm^{-2} for the Base Case, and 400 mA cm^{-2} for the More Optimal Case. We later vary this value (figures 9 - 10) to show how it affects the cell performance. We are interested in separating the losses that arise from mass transport and those that arise from activation of the charge-transfer reaction. In order to do this, we define the mass transport overpotential, η_{MT}, as the total bromine overpotential (η_{Br}, obtained from Equation 22) minus the activation overpotential (η_{Br}', obtained from Equation 21, applied to bromine instead of hydrogen):

$$\eta_{MT} \equiv \eta_{Br} - \eta_{Br}' \qquad (23)$$

To find η_{MT}, we determined the flux of reactants to the surface (and products away from it). The diffusive flux, J (in mol cm^{-2} s^{-1}) is given by

$$J = -D \frac{dC}{dx} \approx -D \frac{\Delta C}{\Delta x}, \qquad (24)$$

where in the second expression we have made the quasi-

stationary, linear concentration gradient approximation across the bromine-side electrode. D is the diffusion coefficient (in $cm^2\ s^{-1}$). For diffusion of Br_2(aq), we label the diffusion coefficient D_{Br_2}. Δx is equal to ε, the diffusion layer thickness, and ΔC is the concentration difference across the thin film, namely $C_O^s(i) - C_O^{bulk}$ (in mol cm^{-3}). For each mole of Br_2 that diffuses to the electrode surface to react, $2F$ coulombs of electrons pass through the external circuit for bromine reduction. Thus, the flux is expressed as a current density according to $i=2FJ\cdot1000$, where the factor of 1000 is necessary for conversion from A to mA. Equation 24 can be solved for $C_O^s(i)$:

$$C_O^s(i) = C_O^{bulk} - \frac{\varepsilon}{2FD_{Br_2}}\frac{i}{1000}. \quad (25)$$

Ideally, data for D_{Br_2} as a function of temperature, Br_2 concentration, and HBr concentration would be used here, but such data do not appear to exist in the literature. As a result, we rely on a modified version of the Wilke-Change correlation (Wilke & Chang, 1955) provided by Reddy and Doraiswamy (1967) for estimating liquid diffusivities. The following equation is used to calculate D_{Br_2} in pure water (based on Equation 2 in Reddy *et al.*):

$$D_{Br_2} = 10^{-7}\cdot\frac{\left(MW_{H_2O}\right)^{\frac{1}{2}}T}{\mu\left(V_1\right)^{\frac{1}{3}}\left(V_2\right)^{\frac{1}{3}}} \quad (26)$$

where MW_{H_2O} is the molecular weight of water (18.0153 g mol^{-1}), μ is the viscosity of the solution (in centipoise), V_1 is the molecular volume of the pure solute (in $cm^3\ mol^{-1}$), and V_2 is the molecular volume of the solvent, i.e. water (in $cm^3\ mol^{-1}$). In the case of bromine, V_1 is equal to 53.2 $cm^3\ mol^{-1}$, and for water V_2 is 18.9 $cm^3\ mol^{-1}$ (Wilke & Chang, 1955). The viscosity itself is temperature dependent, and can be calculated for H_2O using Equation 11 from Laliberté (2007):

$$\mu = \frac{T+246}{(0.05594T+5.2842)T+137.37} \quad (27)$$

Plugging Equation 27 into Equation 26 provides an expression for the diffusivity of Br_2 in H_2O. At 25 °C, the calculated diffusion coefficient for Br_2 is 1.42 x 10^{-5} $cm^2\ s^{-1}$. We assume that this diffusivity is independent of the HBr concentration. For low concentrations of either HBr or Br_2, this assumption is reasonable. As the concentrations get higher and complexed species like Br_3^- and Br_5^- become more prevalent, then the diffusivity calculated here likely overestimates the real value for D_{Br_2}. Bromine speciation can be very important to a system like this, particularly in the high concentration regimes, where Br_3^- and Br_5^- concentrations are likely significant. There is also the possibility of bromine hydrolysis, which is discussed elsewhere (Beckwith, Wang, & Margerum, 1996; Liebhafsky, 1934). In principle, Br_3^- and Br_5^- formation would affect both the electrode kinetics and mass transport through the system. There is some evidence that Br_3^- reduction occurs via a mechanism where Br_3^- first forms Br_2, which Br_3^- is in rapid equilibrium with, followed by reduction of Br_2 (Mastragostino & Gramellini, 1985). If this equilibrium is fast, then Br_3^- formation will likely have little effect on the observed electrode kinetics. The effect on transport will likely be more pronounced: as the concentrations of Br_3^- and Br_5^- increase, the mass transport limit will be adversely affected, as these species will have lower diffusion coefficients than that of Br_2. This is an important consideration, and future modeling efforts that involve a more complex mass transport model will need to account for such effects. We model the bromide mass transport in a similar way to the bromine transport, with a few key differences. As Br_2 is reduced at the electrode, Br^- is produced and the local concentration, $C_R^s(i)$, increases. Protons also enter through the electrode at the same flux as the bromide is generated. As the concentrations increase at the electrode surface, the concentration gradient generates a diffusive flux of Br^- and H^+ away from the electrode. The surface concentration is then modeled by:

$$C_R^s(i) = C_R^{bulk} + \frac{\varepsilon}{FD_{Br^-}}\frac{i}{1000} \quad (28)$$

Note that the sign has changed (relative to Equation 25) because positive fluxes of Br^- require negative current densities. Also, a factor of two is absent from the second term because there is one charge per bromide ion, as opposed to two charges per bromine molecule in the previous case. To estimate the diffusivity of Br^- in solution, we use Equations 26 and 27, with only the value of V_1 changing – to 27 $cm^3\ mol^{-1}$ for Br^-. At 25 °C, the calculated value for D_{Br^-} is 1.78 x 10^{-5} $cm^2\ s^{-1}$. The last term to discuss here is the diffusion layer thickness $\Delta x = \varepsilon$ from Equation 24. This is the primary factor in determining the mass transport characteristics of the cell. A smaller value for ε results in larger diffusive fluxes of reactant to the surface, and therefore higher limiting current densities. In a real cell, the value for ε is a complicated function of the electrode and flow channel geometry and solution flow rates. For a simplified model, we assume that the value for ε is at most the thickness of the electrodes (i.e. approximately 125 μm) for the Base Case. This is akin to a cell setup where solution is being pumped over a porous, planar electrode and the limiting step in mass transport is diffusion of the active species through the electrode. Of course, real cells often add convective transport to this as well (by using interdigitated flow fields, for example), and so the effective values for ε seen are much lower than the electrode thickness. A lower bound on ε can be estimated using fluid mechanics. Assuming a porous, fibrous electrode with fiber diameters

on the order of 10 μm, and assuming that the diffusion layer thickness is set by the formation of a boundary layer across these fibers, the thickness of this layer can be estimated using the Blasius solution for laminar flow over flat plates:

$$\varepsilon \approx 4.91\left(\frac{\nu x}{u_0}\right)^{\frac{1}{2}} \quad (29)$$

where ν is the kinematic viscosity, x is the distance downstream from the beginning of the boundary layer, and u_0 is the free velocity. Using reasonable values for each of these parameters that result in the lowest possible ε (ν = 0.3 x 10^{-6} m^2 s^{-1}, x = 10 μm, and u_0 = 0.1 m s^{-1}), a value of ε = 25 μm is found. Therefore, in this model, we set ε to 125 μm for the Base Case, where the diffusion layer is the entire thickness of the electrode, and to 25 μm for the More Optimal Case, where the diffusion layer is set by the formation of a boundary layer across the electrode fibers. In the exploration of OPs reported here, the cell temperature is varied from 5 ˚C to 75 ˚C, and the HBr(aq) molarity from 0.5 M to 7 M. The Br_2(aq) concentration is always held equal to the HBr(aq) concentration. This is effectively modeling a cell in which there is a large reservoir of $Br_2(\ell)$ sitting underneath an aqueous mixture of Br_2(aq) in HBr(aq). In general, as the HBr(aq) concentration increases as the cell is discharged, the solubility of Br_2 in the upper aqueous phase increases, both HBr(aq) and Br_2(aq) concentrations in the upper phase increase, and the $Br_2(\ell)$ reservoir is depleted. This continues until the $Br_2(\ell)$ reservoir is gone, and then the Br_2(aq) concentration begins to fall until it approaches zero. This model assumes that the $Br_2(\ell)$ reservoir is never completely consumed, so that the Br_2(aq) concentration continuously increases with the HBr(aq) concentration in discharge mode. In charge mode, we make the same assumption – that an upper aqueous phase of Br_2(aq) and HBr(aq) is in equilibrium with a $Br_2(\ell)$ reservoir – so that, as the HBr(aq) concentration falls in the aqueous phase, so does the Br_2(aq) concentration.

2. RESULTS AND DISCUSSION

The model calculates the cell potential according to Equation 4, accounting for the various effects of concentration, temperature, and pressure on each of the overpotentials. The Base Case engineering parameters have the following values: hydrogen electrode exchange current density i_0^H = 250 mA cm^{-2}, Br_2 electrode exchange current density i_0^{Br} = 40 mA cm^{-2}, membrane thickness l=125μm, diffusion layer thickness ε = 125 μm, and H_2 gas pressure p_{H_2}=1 atm. The More Optimal Case EPs have the following values: i_0^H = 600 mA cm^{-2}, i_0^{Br} = 400 mA cm^{-2}, l = 25 μm, ε = 25 μm, and H_2 gas pressure p_{H_2}=5 atm. Figure 4 shows a directs comparison of the cell potential vs. current density and power density vs. current density for the Base Case and the More Optimal Case. These calculations were done at 75 ˚C and 2 M HBr/Br_2, which are the operating parameters where the cell voltage efficiency is highest for both cases (see figure 7). The maximum power density seen for the Base Case under these operating conditions approaches 530 mW cm^{-2}, with a limiting current density near 1200 mA cm^{-2} in galvanic mode. For the More Optimal Case in galvanic mode, the maximum power density is 2760 mW cm^{-2}, with a limiting current density just above 6000 mA cm^{-2}. In electrolytic mode, the limiting current density for the Base Case is about -750 mA cm^{-2}, and, for the More Optimal Case, the limiting current density in electrolytic mode is -3770 mA cm^{-2}. The limiting current densities are lower in the electrolytic direction because, when a mole of Br^- is oxidized, it frees 1 mole of electrons. In galvanic mode, when a mole of Br_2 is reduced, it liberates 2 moles of electrons. Thus, despite the higher diffusivity of Br^- in solution than Br_2, the limiting current density is actually lower in electrolytic mode.

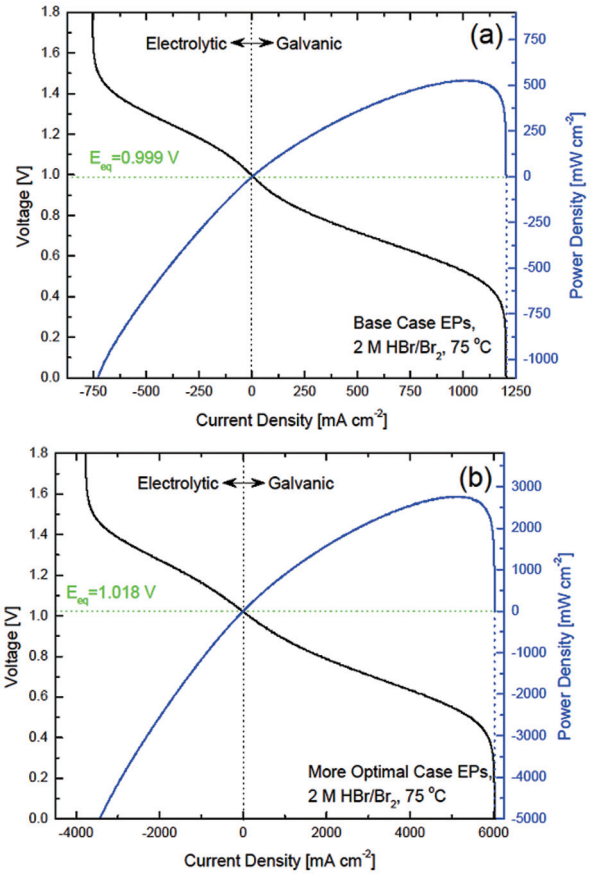

Figure 4
Voltage vs. Current Density (Black) and Power Density vs. Current Density (Blue) for the (a) Base Case and (b) More Optimal Case, both at 75 ˚C and 2 M HBr/Br_2 (the Operating Conditions that Provide the Highest Voltage Efficiency Cell)
The equilibrium potential is indicated with a green dotted horizontal line, and both galvanic and electrolytic operation are shown.

Figure 5 shows calculated cell potentials for the (a) Base Case at 25 ˚C and 2 M HBr/Br_2, (b) More Optimal Case at 25 ˚C and 2 M HBr/Br_2, and (c) More Optimal Case at 75 ˚C and 2 M HBr/Br_2. The latter represents the conditions under which the cell efficiency is highest. The contributions of each of the individual losses are indicated as well. The horizontal dotted line shows the cell equilibrium potential. Mass transport losses are minimal at relatively low current densities while, as the limiting current density is approached, mass transport losses dominate – until the cell potential is finally reduced to zero. It is also important to note that, at low current densities, the dominant loss for both the Base and More Optimal Cases is the bromine electrode overpotential. The relative contributions of the losses are not vastly different between the Base Case and More Optimal Case: the hydrogen electrode activation overpotential is relatively more important in the More Optimal Case than in the Base Case because, in the More Optimal Case, the values of the bromine and hydrogen electrode exchange current densities are nearer one another. Comparing figures 5b and 5c, the primary effects of raising the cell temperature are to increase the limiting current density due to enhanced reactant diffusivities and to improve the membrane conductivity, thereby reducing ohmic losses through the cell. The electrode kinetics becomes the most important factor affecting cell performance for the More Optimal Case cell operating under ideal conditions, indicating that electrode design is going to be an important factor in achieving high performance in these devices.

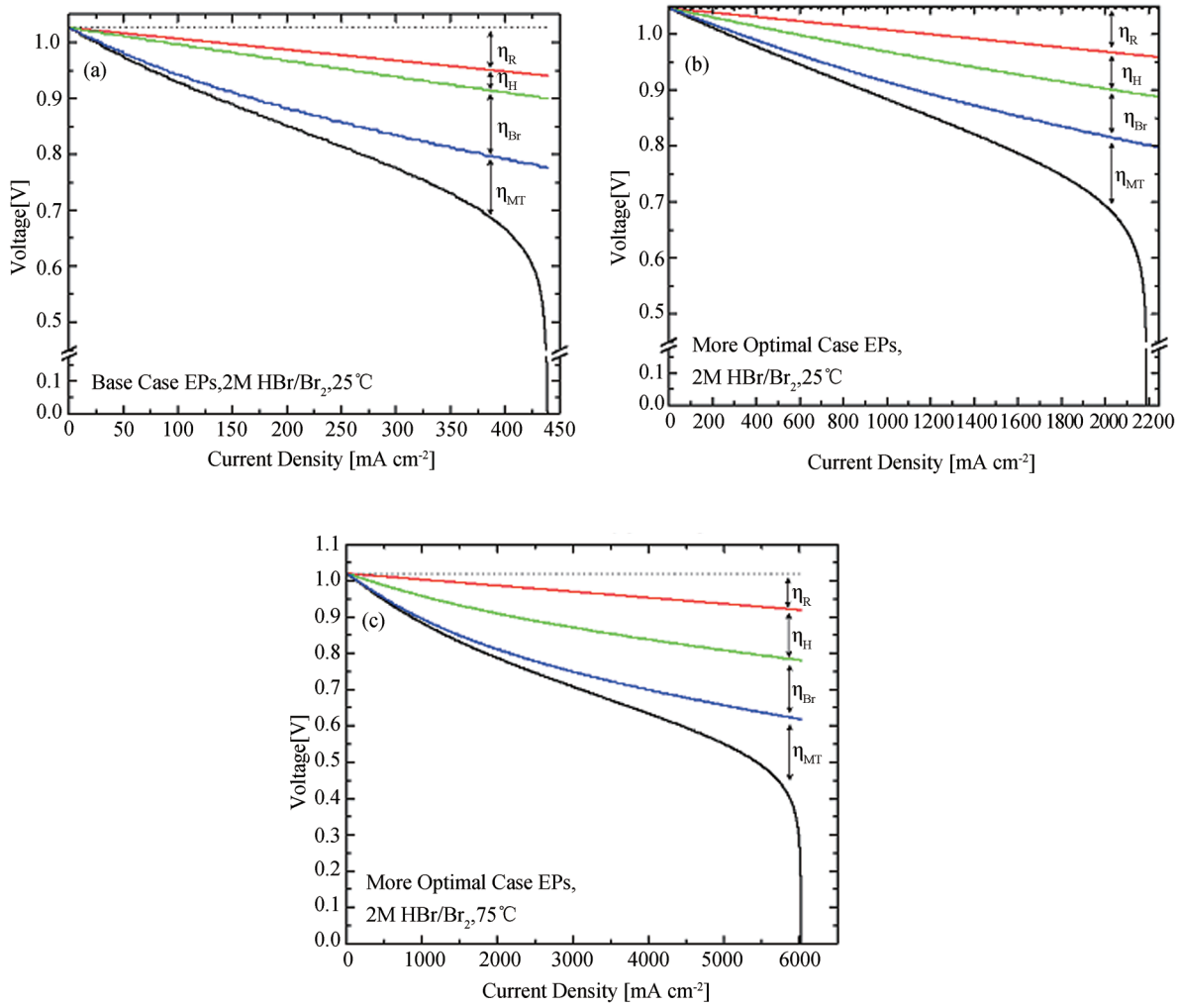

Figure 5
Voltage vs. Current Density for the (a) Base Case at 25 ˚C and 2 M HBr/Br_2, (b) More Optimal Case at 25 ˚C and 2 M HBr/Br_2, and (c) More Optimal Case at 75 ˚C and 2 M HBr/Br_2 (the Operating Conditions Where the Cell Efficiency is Highest)

The two most relevant performance characteristics are the cell efficiency-vs.-current-density function and the maximum cell power density. On one hand, high cell efficiency is paramount for energy storage devices because lost energy is lost revenue. It is imperative that a storage device be able to operate at high efficiencies at

reasonable current densities. On the other hand, operating at higher power densities reduces the capital cost for a given power-delivery capability, because one may buy less cell area for an equivalent power. The maximum power density also permits a determination of the minimum membrane area (and associated cost) necessary to achieve a required system power. In any real storage system (used to levelize wind power, for example), the cell operates over a distribution of current densities, constantly ramping up and down, depending on how much power is being generated by the turbines. Thus, both the maximum power density and the cell efficiency are important, so we explore both of these characteristics in this model. It is worth noting too, that, generally speaking, increasing the maximum power results in an efficiency increase over the entire current density range. It is important, however, to keep in mind that the relative contributions of the individual loss mechanisms to the total loss may be significantly different at peak power than at high efficiency. Varying the cell operating parameters of temperature and electrolyte composition drastically affects the cell performance, as demonstrated in figure 6. The concentrations of HBr and Br_2 are varied for a cell operating at 25 ˚C with Base Case EPs in figure 6a, and with the More Optimal Case EPs in figure 6c. Increasing the concentrations leads to increased limiting current densities, but also, in accordance with the Nernst equation, leads to decreased equilibrium potentials. Note that in the 6 M HBr/Br_2 case for both figures 6a and 6c, the mass transport limited current density is never actually reached: the cell potential goes to zero largely due to ohmic losses in the membrane. The behavior of a cell operating at 1 M HBr/Br_2 over three different temperatures is shown in figure 6b for a cell with Base Case EPs, and in figure 6d for a cell with More Optimal Case EPs. Increasing temperature leads to slightly reduced equilibrium potentials, but it also leads to significantly higher limiting current densities. All of the individual losses are reduced by increasing temperature, so, for this type of cell, higher temperatures always lead to higher voltage efficiencies.

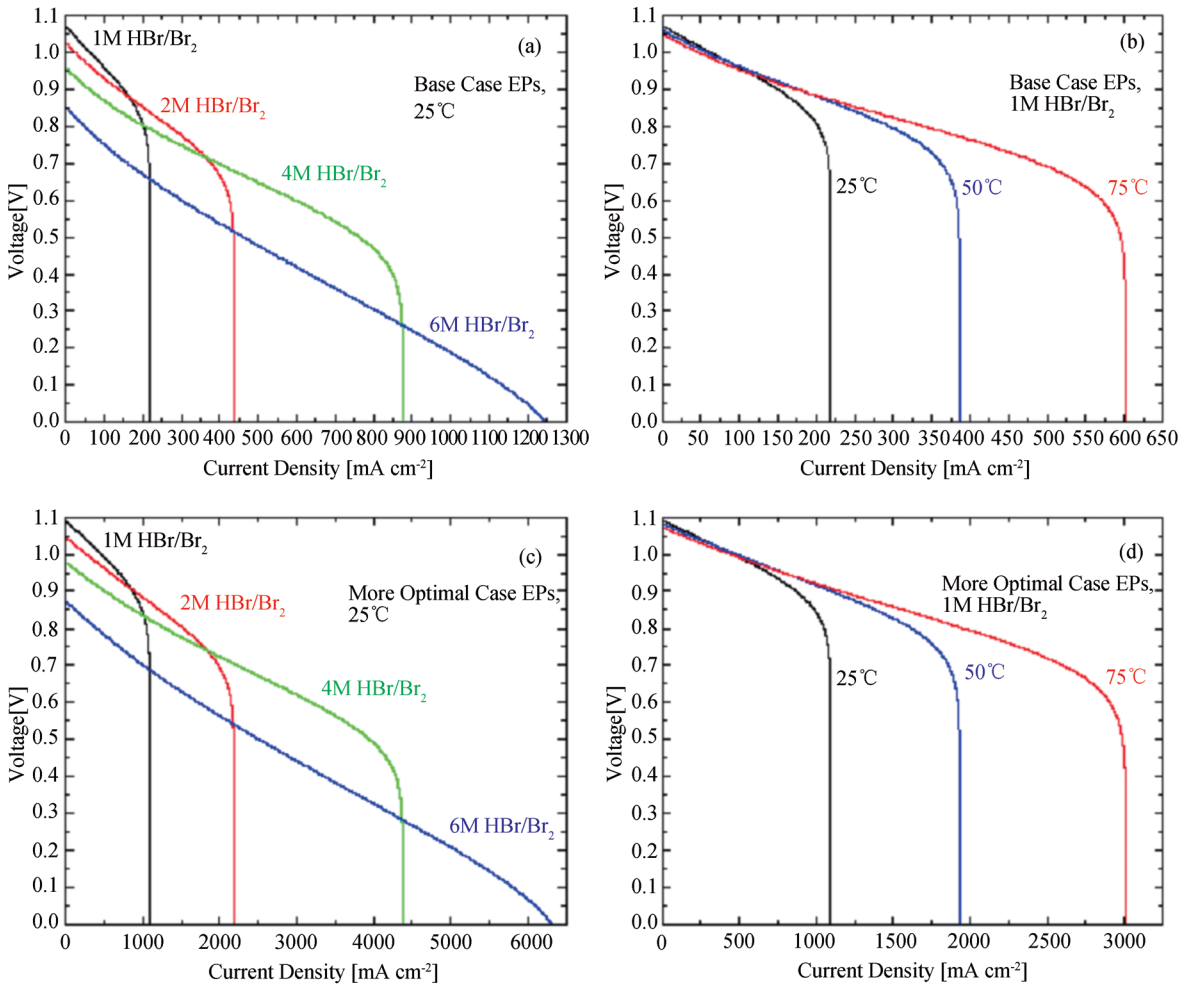

Figure 6
Voltage vs. Current Density over a Range of Operating Conditions: (a) Base Case EPs, 25 ˚C, Varying Concentration; (b) Base Case EPs, 1 M HBr/Br_2, Varying Temperature; (c) More Optimal Case EPs, 25 ˚C, Varying Concentration; (d) More Optimal Case EPs, 1 M HBr/Br_2, Varying Temperature

Figure 7 shows how the maximum power density and galvanic power density at 90% voltage efficiency vary over the entire range of operating parameters explored, calculated using the Base Case EPs for the top row of the plots and the More Optimal Case EPs for the bottom row. For each combination of temperature and concentration (denoted by the points of intersection in the overlaid grid), a voltage vs. current density curve was calculated, similar to figure 4, and, from this, a maximum power density and a galvanic power density at 90% voltage efficiency were calculated. The values of each of these were then plotted for every combination of temperature and concentration, forming the surfaces shown in figure 7. As is evident from the figure, the surfaces calculated for the Base Case and the More Optimal Case have a very similar shape. Furthermore, the effect of temperature is clear: higher temperatures lead to higher maximum power densities and higher power densities at 90% voltage efficiency. This is because an increased temperature reduces all of the individual losses. The effect of concentration is more complex, but, in general, the dominant effect is the membrane conductivity. At low temperatures, the conductivity has a local maximum near 4 M. As the temperature increases, this maximum shifts to lower molarities, and, at 75 ˚C, the conductivity has an absolute maximum near 2 M. This explains the shift of the peak power density for a given temperature to lower molarities as the temperature is increased.

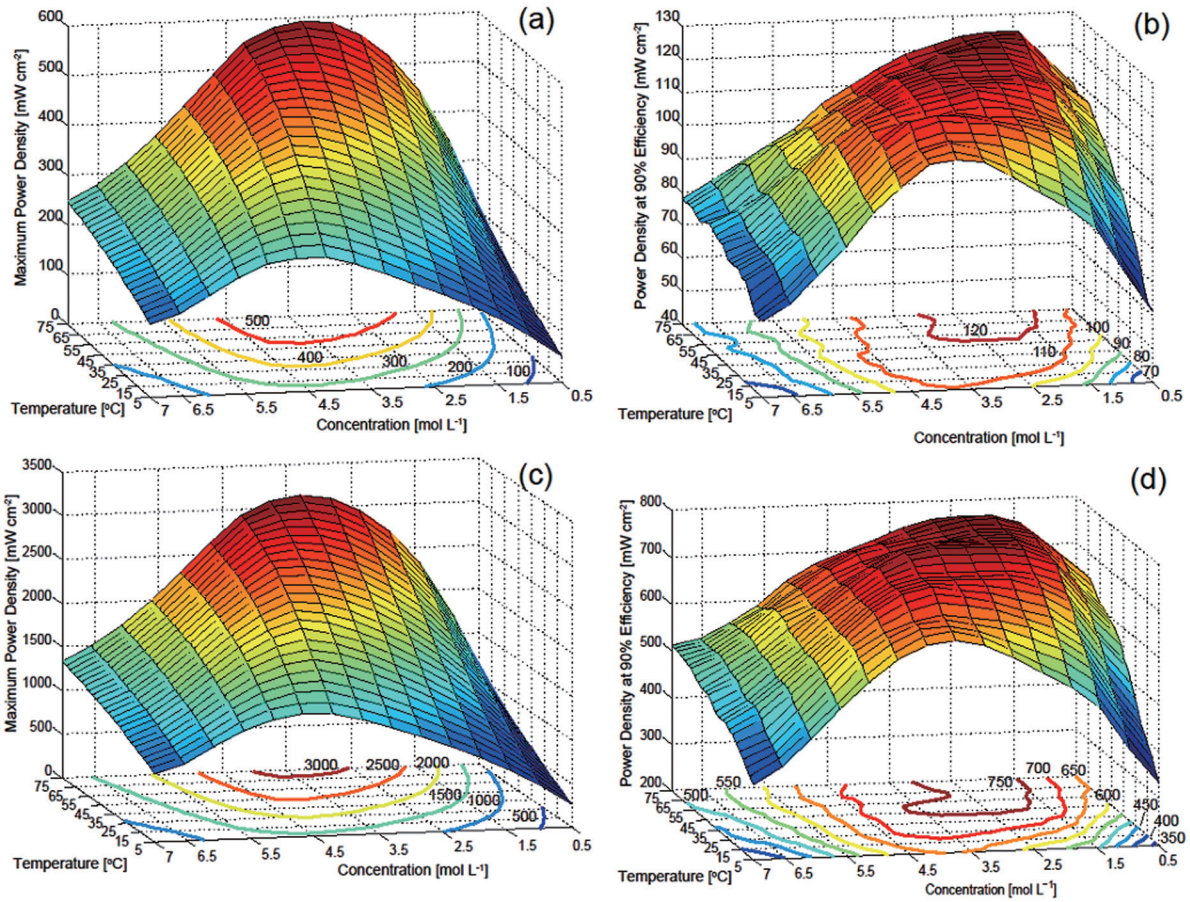

Figure 7
(a) Maximum Power Density vs. Temperature and Concentration for the Base Case, (b) Power Density at 90% Voltage Efficiency vs. Temperature and Concentration for the Base Case, (c) Maximum Power Density vs. Temperature and Concentration for the More Optimal Case, and (d) Power Density at 90% Voltage Efficiency vs. Temperature and Concentration for the More Optimal Case

These were calculated using the Base Case EPs for (a) and (b): H_2 electrode exchange current density i_0^H = 250 mA cm^{-2}, Br_2 electrode exchange current density i_0^{Br} = 40 mA cm^{-2}, membrane thickness l = 125 μm, diffusion layer thickness ε = 125 μm, H_2 gas pressure p_{H_2} = 1 atm and More Optimal Case EPs for (c) and (d): H_2 electrode exchange current density i_0^H = 600 mA cm^{-2}, Br_2 electrode exchange current density i_0^{Br} = 400 mA cm^{-2}, membrane thickness l = 25 μm, diffusion layer thickness ε = 25 μm, H_2 gas pressure p_{H_2} = 5 atm. Contour lines are projected onto the temperature-concentration plane. The "jaggedness" in (b) and (d) is due to computational mesh-size limitations and is not a real effect.

Figure 8 shows the cell voltage efficiency as a function of the galvanic power density under a variety of operating conditions for both the Base Case and the More Optimal Case. The dotted regions of each curve indicate areas of undesirable operation, as one would always choose to operate at the highest efficiency for a given power density. Notice how, for the Base Case, the electrolyte composition has little effect on the predicted cell

performance at 90% efficiency: only when the maximum power densities are approached do significant differences become evident. For the More Optimal Case running at 75 ˚C, the 1 M and 2 M curves are indistinguishable at high efficiencies, as both the membrane resistance and mass transport overpotentials are small there, but the curves do become quite different as the maximum power densities are approached. The mass transport limitation sets in first for the lower concentration. The 4 M curve is considerably worse over the majority of the efficiency range of interest, due to decreased membrane conductivity at this high acid concentration (see figure 3); however, the high concentration forestalls the mass transport limitation, thereby reaching the highest power density.

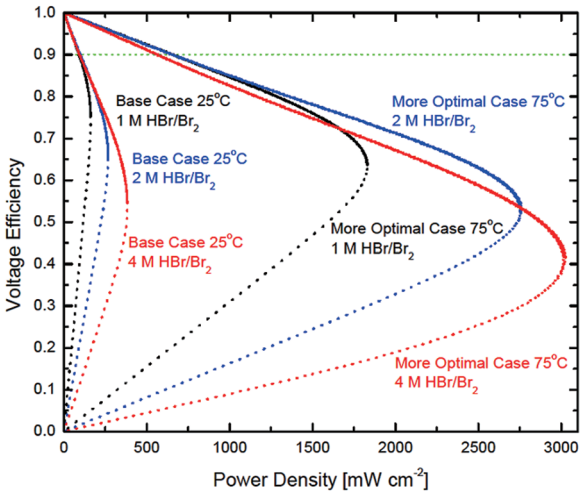

Figure 8
Voltage Efficiency vs. Power Density Under a Variety of Operating Conditions for Both the Base Case and the More Optimal Case
The dotted portions of the curves indicate regions of undesirable operation, as the efficiency decreases with decreasing power density. The horizontal line indicates 90% voltage efficiency.

In figure 9, we report the variation of the maximum peak power density (the height of the highest point in figure 7) as each of the engineering parameters (other than the hydrogen exchange current density, which is fixed at i_0^H = 250 mA cm^{-2}) is varied away from the Base Case while keeping the other four EPs fixed. Because higher temperatures always lead to higher cell efficiencies, the black (upper) dots were calculated at 75 ˚C, and the red (lower) ones at 5 ˚C. The black dots represent operation of the cell at 75 ˚C and the HBr/Br$_2$ concentration that results in the highest peak power density. The red (lower) dots represent operation at 5 ˚C and the HBr/Br$_2$ concentration that results in the lowest peak power density. In figure 9a we varied i_0^{Br} from the certainly attainable value of 1 mA cm^{-2}, to the likely unattainable value of 1000 mA cm^{-2}. For this set of EPs, there are significantly diminishing returns for efforts to increase i_0^{Br} beyond about 100 mA cm^{-2}, but decreasing i_0^{Br} below the Base Case causes a substantial degradation in performance. In figure 9b we show how performance increases with decreasing membrane thickness, due to decreasing membrane resistance. Nafion is currently commercially available in thicknesses from 25 to 250 μm. In figure 9c we show that the power performance declines considerably for large values of the diffusion layer thickness ε; this occurs because of small limiting current densities. Engineering a cell with as low a value of ε as possible is critical to achieving a high power density. Lastly, in figure 9d, we show how the cell performance depends on the pressure of H_2 gas. Higher pressure gives a modest boost to the open circuit potential, but the gains to the maximum power density are minimal. Thus, it is apparent that increasing the H_2 pressure only has a modest effect on the cell performance.

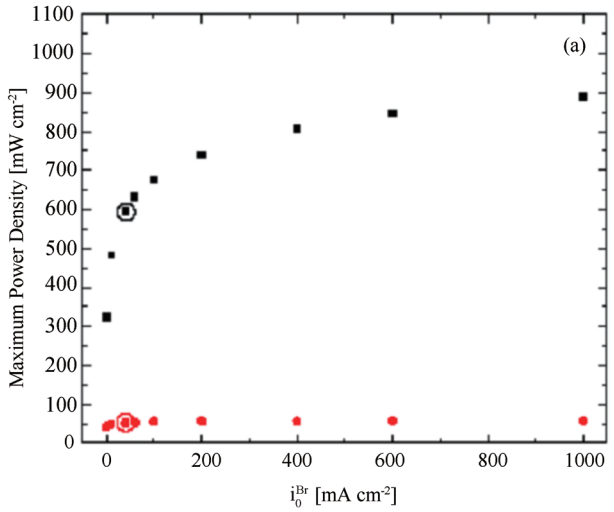

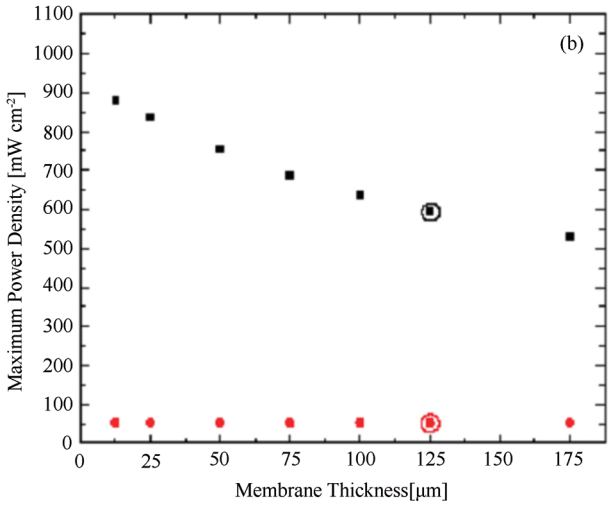

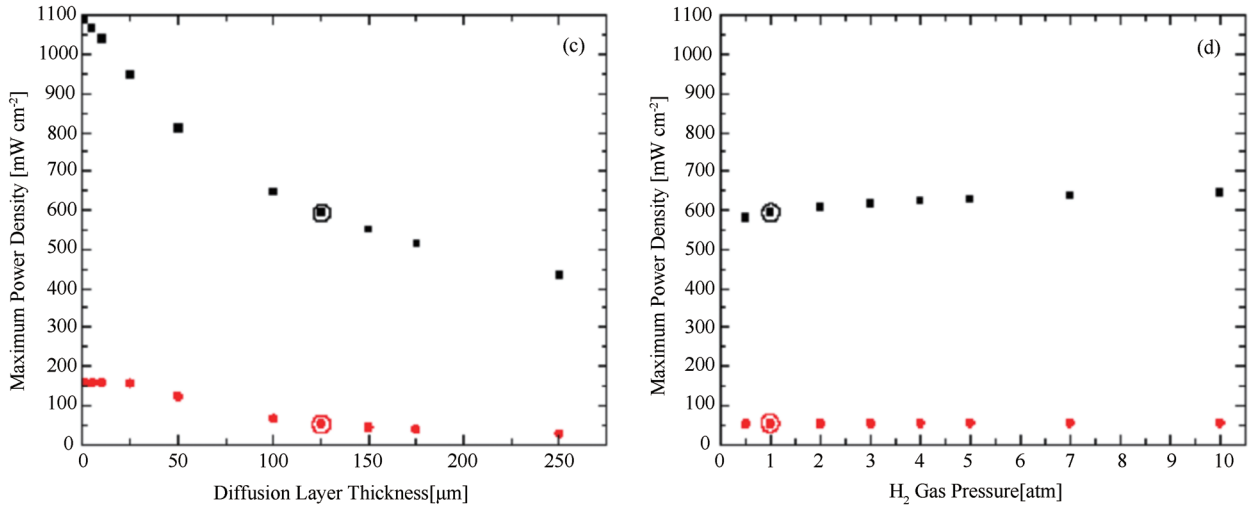

Figure 9
Dependence of Performance on Deviation from the Base Case Engineering Parameters
Maximum power densities are displayed as a function of each engineering parameter with the others held at their base values: H_2 electrode exchange current density i_0^H = 250 mA cm^{-2}, Br_2 electrode exchange current density i_0^{Br} = 40 mA cm^{-2}, membrane thickness l = 125 μm, diffusion layer thickness ε = 125 μm, H_2 gas pressure p_{H_2} = 1 atm. In (a) i_0^{Br} is varied, in (b) l is varied, in (c) ε is varied, and in (d) H_2 pressure is varied. The Base Case is circled in each plot. The black (upper) dots represent operation of the cell at 75 ˚C and the HBr/Br_2 concentration that results in the highest peak power density. The red (lower) dots represent operation at 5 ˚C and the HBr/Br_2 concentration that results in the lowest peak power density. The pairs of dots effectively bracket the expected cell performance over the entire range of temperatures and HBr/Br_2 concentrations explored in this study.

While figure 9 focuses on the effects on the peak power density of varying the individual EPs, it is also important to understand how the cell power density at high efficiency varies with the EPs. The variations are not necessarily similar because different contributions dominate the loss at peak power and at high efficiency. From figure 5, it is clear that the dominant loss at 90% galvanic efficiency is the bromine activation overpotential. Thus, varying the bromine electrode exchange current density should have the largest effect on cell performance at 90% efficiency. Figure 10a confirms this expectation. Figures 10b, 10c, and 10d show that the Nafion thickness, diffusion layer thickness, and H_2 pressure are much less critical to cells operating at high efficiencies: gains here only have a modest effect on cell performance.

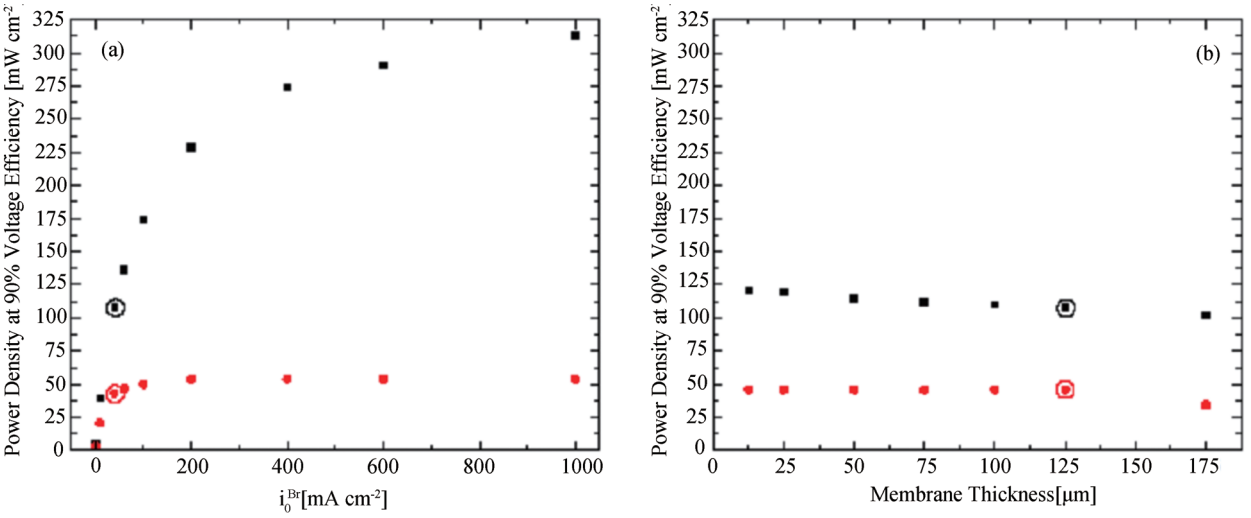

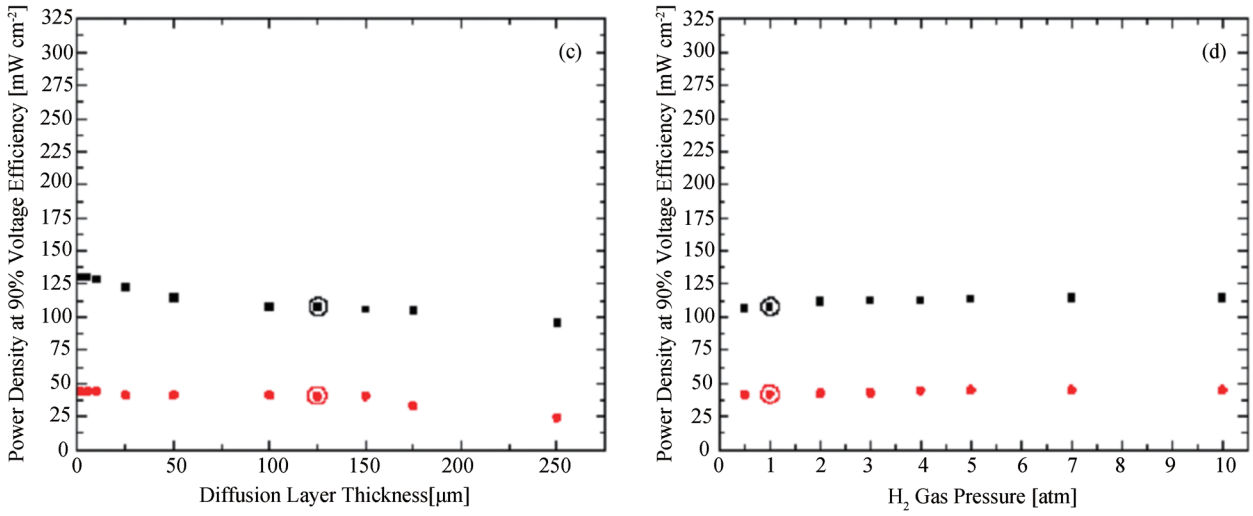

Figure 10
Dependence of Performance on Deviation from the Base Case Engineering Parameters
Power density at 90% voltage efficiency is displayed as a function of each engineering parameter with the others held at their base values: H_2 electrode exchange current density i_0^H = 250 mA cm^{-2}, Br_2 electrode exchange current density i_0^{Br} = 40 mA cm^{-2}, membrane thickness l = 125 μm, diffusion layer thickness ε = 125 μm, H_2 gas pressure p_{H_2} = 1 atm. In (a) i_0^{Br} is varied, in (b) l is varied, in (c) ε is varied, and in (d) H_2 pressure is varied. The Base Case is circled in each plot. The black (upper) dots represent operation of the cell at 75 ˚C and the HBr/Br_2 concentration that results in the highest peak power density. The red (lower) dots represent operation at 5 ˚C and the HBr/Br_2 concentration that results in the lowest peak power density. The pairs of dots effectively bracket the expected cell performance over the entire range of temperatures and HBr/Br_2 concentrations explored in this study.

Finally, we compare the model results to a recently published experimental report that is sufficiently detailed that a comparison is possible. Kreutzer *et al.* (2012) report on hydrogen-bromine cells that use a commercial electrode with a Pt loading of about 0.55 mg cm^{-2} for the bromine electrode. In figure 11, a fit of our model to a temperature series they collected is shown. Both potential vs. current density and power density vs. current density fits and data from Kreutzer *et al.* are included. The model curves at three different temperatures are shown as solid lines, and the data from Kreutzer *et al.* are indicated using markers (hollow circles for 23 ˚C, hollow triangles for 35 ˚C, and hollow squares for 45 ˚C). The data that are fit were collected at 23 ˚C, 35 ˚C, and 45 ˚C using a 2 M HBr/Br_2 electrolyte, 1.204 atm H_2 pressure (equivalent to 3 psig), and Nafion 212 (50 μm thick). The exchange current density for the Br_2 electrode used is calculated based on experimental results provided in the paper. They measured a Br_2/Br^- exchange current density of 0.3 mA cm^{-2} on flat Pt, and, because the structured electrodes used in the cell have reported surface area enhancement factors of about 556-667 cm^2 of Pt per cm^2 of electrode, this corresponds to an exchange current density for the electrode of 167-200 mA cm^{-2}. A value of 183.5 mA cm^{-2} – the middle of this range – is used for model fitting purposes, and a value of 600 mA cm^{-2} is used for the hydrogen electrode exchange current density. With these EPs held constant, the only free parameter left to fit is the diffusion layer thickness ε. The best fit value for the 45 ˚C curve is 116 μm, slightly under the Base Case value of 125 μm. The model fit is best when ε is permitted to vary, but, in practice, ε should be independent of temperature. Therefore, we use the value of 116 μm for all three curves, which we believe represents a more realistic fitting scenario. This does explain, though, why the fit is better at high current densities for the 45 ˚C data than either of the other two datasets. It appears that the model overestimates the effect of temperature on mass transport. Mathematically, the temperature dependence is encapsulated in Equations 26 and 27, which describe the species diffusivity and viscosity of water, respectively. Having experimental data for the diffusivities of Br_2 and HBr in aqueous mixtures of Br_2 and HBr and data for the viscosities of these solutions at a variety of compositions and temperatures would likely correct this overestimation, as they would account for the various complexing reactions (i.e. formation of Br_3^- and Br_5^-) and species interactions that naturally occur. Despite this, the quality of the fits is reasonable, working particularly well at low overpotentials and in electrolytic mode.

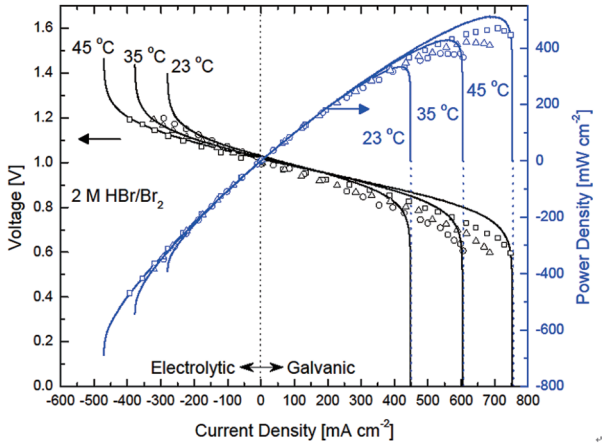

Figure 11
Comparison of Model Fits to Data from Kreutzer *et al.* Collected at 23 ˚C, 35 ˚C, and 45 ˚C Using a 2 M HBr/Br_2 Electrolyte
Model fits are shown using solid lines and data from Kreutzer *et al*. are indicated with markers (hollow circles for 23 ˚C, hollow triangles for 35 ˚C, and hollow squares for 45 ˚C). Values for the engineering parameters used in the model fits are the following: i_0^H = 600 mA cm^{-2}, i_0^{Br} = 183.5 mA cm^{-2}, membrane thickness l = 50 μm, H_2 gas pressure p_{H_2} = 1.2 atm, diffusion layer thickness ε = 116 μm. The only adjustable parameter was ε.

CONCLUSIONS

We developed a model for a PEM-based regenerative hydrogen-bromine fuel cell (rHBFC) including four voltage loss mechanisms: hydrogen electrode activation, bromine electrode activation, bromine electrode mass transport, and ohmic loss through the membrane. We explored a large parameter space by looking at the dependences of each of these losses as a function of two "operating parameters", acid concentration and temperature; and five "engineering parameters", exchange current densities at both electrodes, membrane thickness, diffusion layer thickness, and hydrogen pressure. The model compares well with a recent experimental report of the behavior of a PEM-based hydrogen-bromine cell, particularly in the low current density regime and for electrolytic operation. We project that, with further R&D, a cell of this design could be developed that operates at greater than 90% voltage efficiency at current densities $>$ 700 mA cm^{-2} in both electrolytic and galvanic modes. The maximum power density for a "Base Case" cell is 530 mW cm^{-2} under the best operating conditions, and, for a "More Optimal Case" cell, 2760 mW cm^{-2}. Raising the operating temperature always improves the voltage efficiency, as all the losses explored here are made smaller by increasing the temperature. At 75 ˚C, the membrane conductivity vs. HBr concentration peaks near 2 M. As the temperature is lowered, the conductivity peaks at progressively higher acid concentrations. For a high galvanic power density at 90% voltage efficiency, the only critical engineering parameter is i_0^{Br}: all other EPs have a weak effect on high efficiency operation. For a high peak power density, the most important engineering parameter is the diffusion layer thickness ε. Thus, it is critical for high power density cells that the mass transport behavior be optimized. For values of i_0^{Br} above about 100 mA cm^{-2}, diminishing returns are met in terms of increasing the maximum power density. However, if i_0^{Br} is too small, the maximum power density is severely reduced.

ACKNOWLEDGEMENTS

We thank Dr. Trent M. Molter for helpful discussions. One of us (B.H.) was supported by an NSF Graduate Research Fellowship. We also acknowledge Jason Rugolo for earlier work on electrochemical systems modeling that directly benefited this work.

REFERENCES

[1] Mellentine, J. A., Culver, W. J., & Savinell, R. F. (2011). Simulation and Optimization of a Flow Battery in an Area Regulation Application. *Journal of Applied Electrochemistry*, *41*(10), 1167-1174.

[2] Eyer, J., & Corey, G. (2010). *Energy Storage for the Electricity Grid: Benefits and Market Potential Assessment Guide*. Sandia Report.

[3] Rugolo, J., & Aziz, M. J. (2012). Electricity Storage for Intermittent Renewable Sources. *Energy & Environmental Science*, *5*, 7151-7160.

[4] Kondoh, J., Ishii, I., Yamaguchi, H., & Murata, A. (2000). Electrical Energy Storage Systems for Energy Networks. *Energy Conversion & Management*, *41*, 1863-1874.

[5] Ibrahim, H., Ilinca, A., & Perron, J. (2008). Energy Storage Systems-Characteristics and Comparisons. *Renewable and Sustainable Energy Reviews*, *12*(5), 1221-1250.

[6] Weber, A. Z., Mench, M. M., Meyers, J. P., Ross, P. N., Gostick, J. T., & Liu, Q. (2011). Redox Flow Batteries: a Review. *Journal of Applied Electrochemistry*, *41*(10), 1137-1164.

[7] Nguyen, T., & Savinell, R. F. (2010). Flow Batteries. *Electrochemical Society Interface*, 54-56.

[8] Anderson, E., Taylor, E., Wilemski, G., & Gelb, A. (1994). A High Performance Hydrogen/Chlorine Fuel Cell for Space Power Applications. *Journal of Power Sources*, *47*(3), 321-328.

[9] Chin, D., Yeo, R., McBreen, J., & Srinivasan, S. (1979). An Electrochemically Regenerative Hydrogen-Chlorine Energy Storage System. *Journal of The Electrochemical Society*, *126*(5), 713-720.

[10] Gileadi, E., Srinivasan, S., Salzano, F., Braun, C., Beaufrere, A., Gottesfeld, S., Nuttall, L., & Laconti, A. (1977). An Electrochemically Regenerative Hydrogen-Chlorine Energy Storage System for Electric Utilities. *Journal of Power Sources*, *2*(2), 191-200.

[11] Mondal, S. K., Rugolo, J., & Aziz, M. J. (2011). Alloy Oxide Electrocatalysts for Regenerative Hydrogen-Halogen Fuel Cell. In He, T., Swider-Lyons, K. E., Park, B., and Kohl, P. (Eds.), *MRS Proceedings*.

[12] Rugolo, J., Huskinson, B., & Aziz, M. J. (2012). Model of Performance of a Regenerative Hydrogen Chlorine Fuel Cell for Grid-Scale Electrical Energy Storage. *Journal of The Electrochemical Society*, *159*(2), B133-B144.

[13] Thomassen, M., Bø rresen, B., Hagen, G., & Tunold, R. (2003). H_2/Cl_2 Fuel Cell for Co-Generation of Electricity and HCl. *Journal of Applied Electrochemistry*, *33*(1), 9-13.

[14] Thomassen, M., Sandnes, E., Bø rresen, B., & Tunold, R. (2006). Evaluation of Concepts for Hydrogen-Chlorine Fuel Cells. *Journal of Applied Electrochemistry*, *36*(7), 813-819.

[15] Yeo, R., McBreen, J., Tseung, A., Srinivasan, S., & McElroy, J. (1980). An Electrochemically Regenerative Hydrogen-Chlorine Energy Storage System: Electrode Kinetics and Cell Performance. *Journal of Applied Electrochemistry*, *10*(3), 393-404.

[16] Yeo, R., & Chin, D. (1980). A Hydrogen-Bromine Cell for Energy Storage Applications. *Journal of The Electrochemical Society*, *127*(3), 549-555.

[17] Balko, E., McElroy, J., & Laconti, A. (1981). Halogen Acid Electrolysis in Solid Polymer Electrolyte Cells. *International Journal of Hydrogen Energy*, *6*(6), 577-587.

[18] Livshits, V., Ulus, A., & Peled, E. (2006). High-power H_2/Br_2 Fuel Cell. *Electrochemistry communications*, *8*, 1358-1362.

[19] Kreutzer, H., Yarlagadda, V., & Van Nguyen, T. (2012). Performance Evaluation of a Regenerative Hydrogen-Bromine Fuel Cell. *Journal of The Electrochemical Society*, *159*(7), F331-F337.

[20] Savinell, R., & Fritts, S. (1988). Theoretical Performance of a Hydrogen-Bromine Rechargeable SPE Fuel Cell. *Journal of Power Sources*, *22*(3-4), 423-440.

[21] Zhang, R., & Weidner, J. W. (2011). Analysis of a Gas-Phase Br_2-H_2 Redox Flow Battery. *Journal of Applied Electrochemistry*, *41*(10), 1245-1252.

[22] Lide, D. (2005). *CRC Handbook of Chemistry and Physics* (91st Edition, pp. 5-1 to 5-3). USA: CRC Press.

[23] Lide, D. (2011). *CRC Handbook of Chemistry and Physics* (92nd Edition, pp. 5-80 to 5-89). USA: CRC Press.

[24] Novotný, P., & Söhnel, O. (1988). Densities of Binary Aqueous Solutions of 306 Inorganic Substances. *Journal of Chemical and Engineering Data*, *33*(1), 49-55.

[25] Yeo, R., & McBreen, J. (1979). Transport Properties of Nafion Membranes in Electrochemically Regenerative Hydrogen/Halogen Cells. *Journal of The Electrochemical Society*, *126*(10), 1682-1687.

[26] Baldwin, R. (1987). Electrochemical Performance and Transport Properties of a Nafion Membrane in a Hydrogen-Bromine Cell Environment. NASA Technical Memorandum, 89862.

[27] Sone, Y., Ekdunge, P., & Simonsson, D. (1996). Proton Conductivity of Nafion 117 as Measured by a Four-Electrode AC Impedance Method. *Journal of The Electrochemical Society*, *143*(4), 1254-1259.

[28] Bard, A. J., & Faulkner, L. R. (2001). *Kinetics of Electrode Reactions*. In Electrochemical Methods (pp. 87-136). John Wiley & Sons.

[29] Neyerlin, K., Gu, W., Jorne, J., & Gasteiger, H. (2007). Study of the Exchange Current Density for the Hydrogen Oxidation and Evolution Reactions. *Journal of The Electrochemical Society*, *154*(7), B631-B635.

[30] White, R. E., Lorimer, S. E., & Darby, R. (1983). Prediction of the Current Density at an Electrode at Which Multiple Electrode Reactions Occur Under Potentiostatic Control. *Journal of The Electrochemical Society*, *130*(5), 1123-1126.

[31] Mastragostino, M., & Gramellini, C. (1985). Kinetic Study of the Electrochemical Processes of the Bromine/Bromide Aqueous System on Vitreous Carbon Electrodes. *Electrochimica Acta*, *30*(3), 373-380.

[32] Wilke, C., & Chang, P. (1955) .Correlation of Diffusion Coefficients in Dilute Solutions. *AIChE Journal*, *1*(2), 264-270.

[33] Reddy, K., & Doraiswamy, L. (1967). Estimating Liquid Diffusivity. *Industrial & Engineering Chemistry Fundamentals*, *6*(1), 77-79.

[34] Laliberté, M. (2007). Model for Calculating the Viscosity of Aqueous Solutions. *Journal of Chemical and Engineering Data*, *52*(2), 321-335.

[35] Beckwith, R., Wang, T., & Margerum, D. (1996). Equilibrium and Kinetics of Bromine Hydrolysis. *Inorganic Chemistry*, *35*(4), 995-1000.

[36] Liebhafsky, H. (1934). The Equilibrium Constant of the Bromine Hydrolysis and Its Variation with Temperature. *Journal of the American Chemical Society*, *56*(7), 1500-1505.

